# Amplitude variation with azimuth – PROGRAM AVAz

## Contents



## Overview

***Interpreter-driven anisotropy analysis of azimuthal anisotropy***

Although the VTI component of anisotropy requires specialized software and (if remigration is necessary) access to a large computing facility, simple HTI (or more simply, azimuthal anisotropy) analysis can be conducted by most interpreters with a limited amount of software. There are currently three popular azimuthal anisotropy analysis workflows, often called velocity variation with azimuth (VVAz), amplitude variation with azimuth (AVAz), and frequency variation with azimuth (FVAz). Less commonly, interpreters also analyze changes in elastic impedance variation with azimuth and attenuation (1/*Q*) variation with azimuth.

Although VVAz is critical for seismic imaging, its measurement from prestack time-migrated gathers has fallen out of favor as a horizontal stress measurement in many shale resource plays because it exhibits a topographic overprint (e.g., Rauch-Davies, 2016). In contrast, AVAz and FVAz analyses work well on time-migrated data volumes. There are four key components for such analysis. First, the seismic data need to be acquired using a wide-azimuth survey, such that the target is illuminated in different directions. Second, the interpreter must request the processing company to provide six-to-eight azimuthally limited migrated subvolumes. Because each seismic trace is migrated independently, the cost of generating azimuthally limited volumes is simply the cost of saving the data to additional files and copying the results to a portable disk drive. Unfortunately, if the interpreter does not request such a product as part of the processing workflow, these intermediate products may be erased after the processing results have been delivered. Third, even if the interpreter does not wish to interpret VVAz effects, these effects exist and can result in misaligned reflectors across different azimuths. In such a case, the interpreter must either perform residual moveout, or more simply, must "register" the six to eight volumes by flattening on a reflector adjacent to the target of interest. Fourth, and finally, the interpreter fits the amplitude, peak frequency, elastic impedance, or $Q$ estimate across azimuthally limited sectors by using equations 66 through 71 and using commercial software or a simple scripting language to estimate the azimuthal eccentricity (or intensity) $e$, the azimuth of the maximum anisotropy $\varphi_{max}$, and the reliability of the estimate $R$.

Rueger (1997) defined AVAz as a simple extension of AVO analysis, wherein the latter is a function only of the incident angle $\vartheta$ and provides an intercept $A$ and a slope $B_{iso}$ (Figure 89). If the geology is azimuthally anisotropic, the coefficient $B_{aniso}$ is nonzero, and the variation of amplitude repeats with a periodicity of 180°. Comparing Figure 89 with equation 70 reveals that Trumbo and Rich's (2013) eccentricity value $e$ is equal to Rueger's (1997) term $B_{aniso}\sin^2\vartheta$ for a fixed incident angle $\vartheta$.

## Computation flow Chart

The input to program AVAz are 4, 6, or 8 equally spaced, azimuthally limited migrated volumes which have been "registered" by flattening each volume on a nearby horizon that is easily picked. The input volumes can be one sample thick (i.e. horizon slices) if desired. The output is a measure at each voxel of the degree of amplitude anisotropy, orientation, and confidence of the least-squares fit to the data.

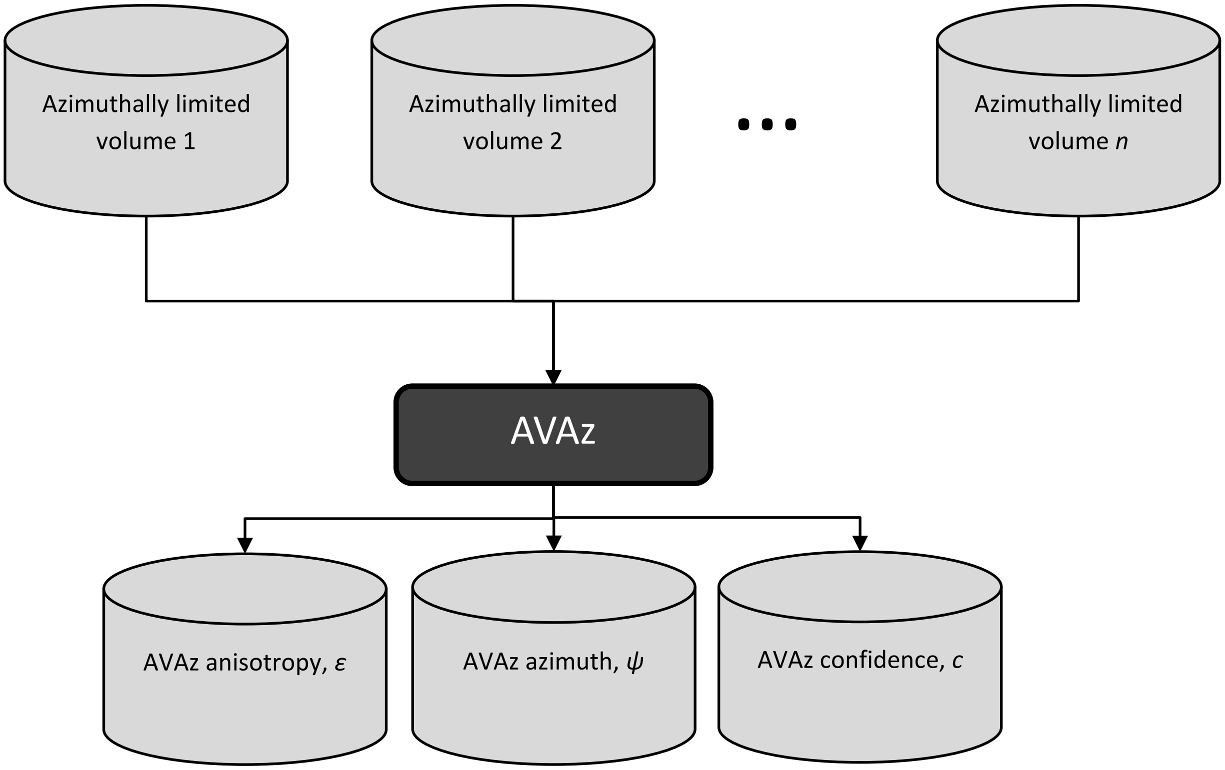
Azimuthally limited volume 1
Azimuthally limited volume 2
...
Azimuthally limited volume *n*
AVAz
AVAz anisotropy, $\varepsilon$
AVAz azimuth, $\psi$
AVAz confidence, $c$

## Output file naming convention

Program **AVAz** will generate the following five output files:

| Output file description | File name syntax |
|---|---|
| Program log information | AVAz_*unique_project_name_suffix*.log |
| Program error and completion information | AVAz_*unique_project_name_suffix*.err |
| Value of azimuthal anisotropy | AVAz_anisotropy_*unique_project_name_suffix*.H |
| Orientation (azimuth) of azimuthal anisotropy | AVAz_azimuth_*unique_project_name_suffix*.H |
| Confidence (accuracy of anisotropy curve to the data) | AVAz_confidence_*unique_project_name_suffix*.H |

where the values in red are defined by the program GUI. The errors we anticipated will be written to the *.err file and be displayed in a pop-up window upon program termination. These errors, much of the input information, a description of intermediate variables, and any software trace-back errors will be contained in the *.log file.

## AASPI Implementation

Program **AVAz** is launched from the **aaspi_util_prestack** GUI from the *Prestack Data Analysis* menu tab:

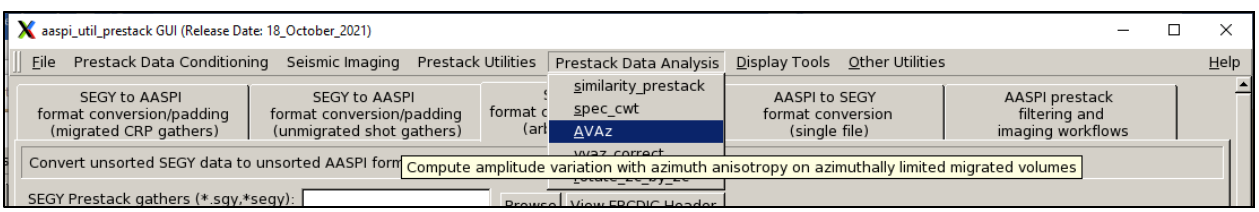


The following GUI appears. (see next page):

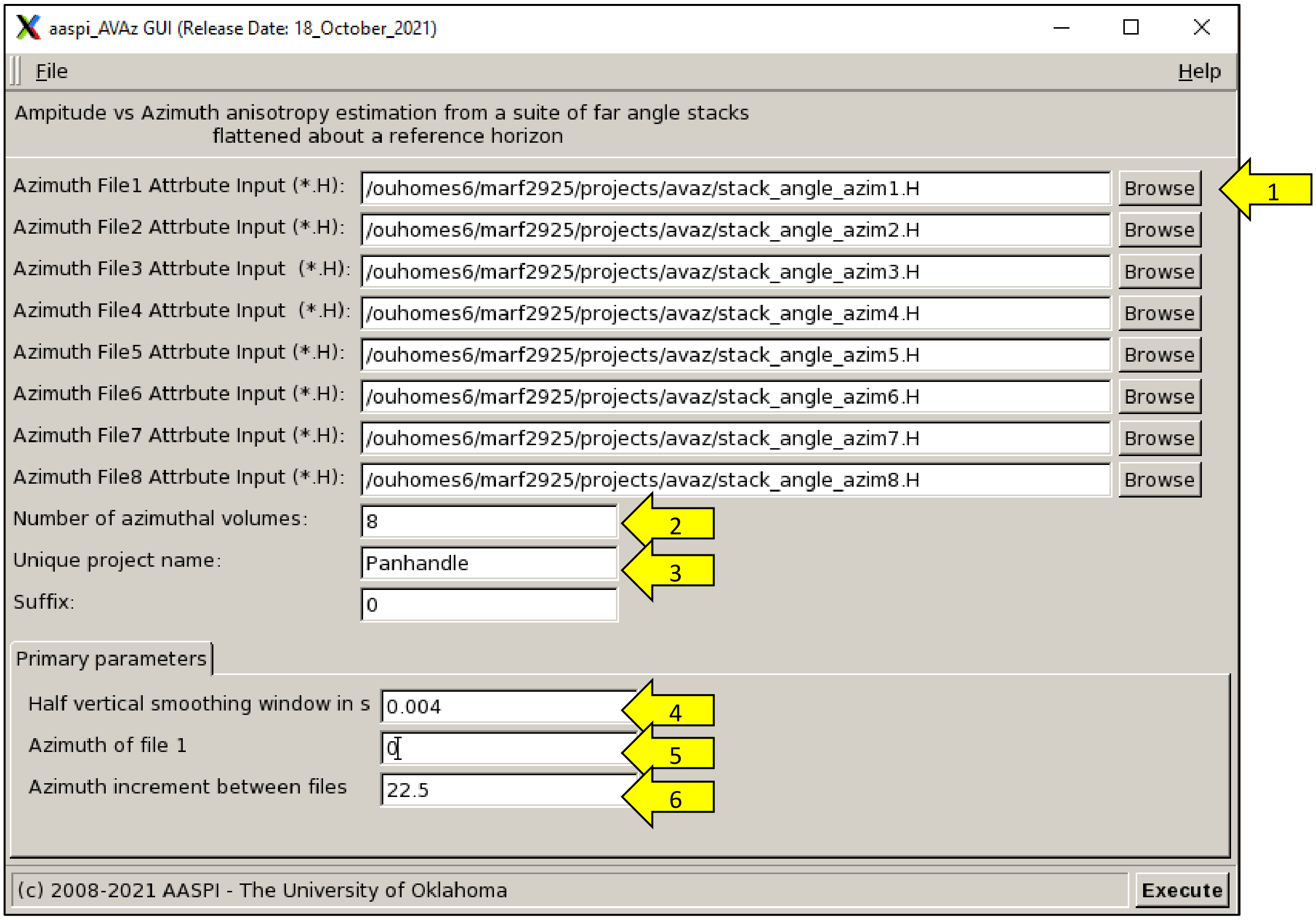


Use the browser to (1) choose four, six, or eight azimuthally limited stacked volumes. The (2) number of the volumes will be augmented as they are entered. As for most AASPI programs, please provide a (3) *Unique project name* and *Suffix*. Then provide (4) a small smoothing window about each sample to help with low amplitude values. The azimuthal volumes are assumed to be equally spaced, beginning at (5) the Azimuth of file 1, with a (6) Azimuth increment between the files. This latter value is computed by assuming the entered files span the range from 0° to 180° such as shown here:

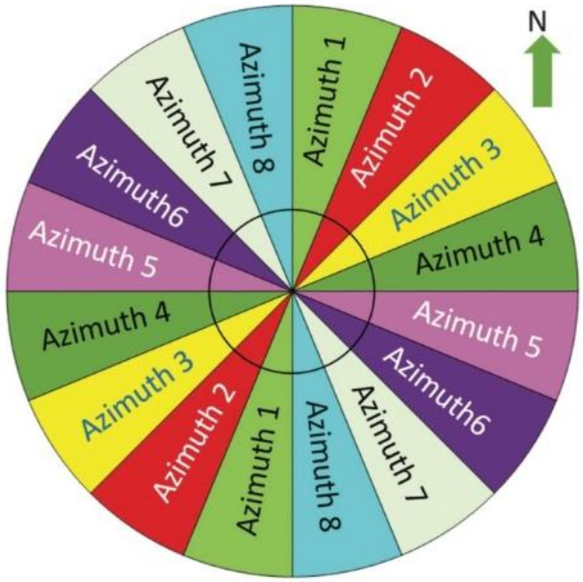


*Eight different azimuthal bins covering the full azimuth range with 22.5° increment.*

**Mathematics of azimuthal variation (from Trumbo and Rich, 2013)**

Assuming an attribute value of the form $A(\varphi)$, which may be traveltime for VVAz analysis, amplitude for AVAz analysis, or frequency for FVAz analysis, Trumbo and Rich (2013) define the azimuthal variation to have the elliptical form

$$A(\varphi) = a\cos^2\varphi + b\cos\sin\varphi + c\sin^2\varphi, \qquad (66)$$

which can then be written as a matrix for measurements made at $N$ discrete azimuths:

$$\begin{pmatrix} A_1 \\ A_2 \\ \vdots \\ A_N \end{pmatrix} = \begin{pmatrix} \cos^2\varphi_1 & \cos\varphi_1\sin\varphi_1 & \sin^2\varphi_1 \\ \cos^2\varphi_2 & \cos\varphi_2\sin\varphi_2 & \sin^2\varphi_2 \\ \vdots & \vdots & \vdots \\ \cos^2\varphi_N & \cos\varphi_N\sin\varphi_N & \sin^2\varphi_N \end{pmatrix} \begin{pmatrix} a \\ b \\ c \end{pmatrix}. \qquad (67)$$

Equation 67has the form **A = TC,** where **A** is a vector of the measured attributes and **C** is a vector of the unknown coefficients, which can be solved using least squares $\mathbf{C} = \left(\mathbf{T}^{\mathbf{T}}\mathbf{T} + \sigma\mathbf{I}\right)^{-1}\mathbf{T}^{\mathbf{T}}\mathbf{A}$ , where **I** is the identity matrix and $\sigma$ is a small value to stabilize the matrix inversion. The direction of maximum amplitude $\varphi_{max}$ aligns with the value max[$A(\varphi)$]. Using this value of symmetry, Trumbo and Rich (2013) show that equation 66can be written as

$$A(\varphi) = \lambda_{max}\cos^2(\varphi - \varphi_{max}) + \lambda_{min}\sin^2(\varphi - \varphi_{max}), \qquad (68)$$

where $\lambda_1$ and $\lambda_2$ are eigenvalues of the matrix **P** defined as

$$\mathbf{P} = \begin{pmatrix} a & b \\ b & c \end{pmatrix}, \qquad (69)$$

and where $\varphi_{max,}$ is the azimuth of the eigenvector associated with the eigenvalue $\lambda_{max}$. The eccentricity $e$ or degree of anisotropy of the best-fit ellipse is given by

$$e = \left[1 - \left(\frac{\lambda_{max}}{\lambda_{min}}\right)^2\right]^{1/2}, \qquad (70)$$

where $e$ ranges between 0 and 1. Trumbo and Rich (2013) then define the reliability $R$ of the azimuthal attribute to be

$$R = \frac{\lambda_{max} - \lambda_{min}}{\left[\sum_{n=1}^{N} \frac{\left[A_n - A(\varphi_n)\right]^2}{4}\right]^{1/2}}. \qquad (71)$$

## Data preparation

If even considering the possible analysis of azimuthal anisotropy, it is critical that your service provider save the azimuthally limited sectors as part of their seismic processing and imaging workflow. Although the service provider may charge a small fee for the increase in data storage and data transfer, for prestack Kirchhoff time migration, there is no additional computation cost in generating azimuthally limited volumes – each shot-receiver pair is migrated separately and will be binned someplace, either in a single stacked volume, in offset-limited bins, in azimuthally limited bins, or in some combination of the latter two. In contrast, once the intermediate data are stacked, there is no going back. Requesting azimuthally limited gathers after the fact requires remigrated the entire data volume.

Most data suffer from velocity variations with azimuth (VVAz). Ideally, such variations are associated with fractures and horizontal stress, but in practice, variations in the overburden, including the surface conditions, contribute to VVAz effects. Even if your data have been properly migrated using a VVAz sensitive algorithm, you will still want to register each azimuthally limited volume. Registering is simply achieved by picking the same, strong, reflector near the target zone on each of the azimuthally limited volumes and flattening the results to the same time. Alternatively, you can extract (and flatten) the data along a picked or phantom horizon, resulting in 3D volumes that are only one sample thick. In the workflow below from Zhang et al. (2020) the data have also been subjected to prestack structure-oriented filtering using AASPI program **sof_prestack**:

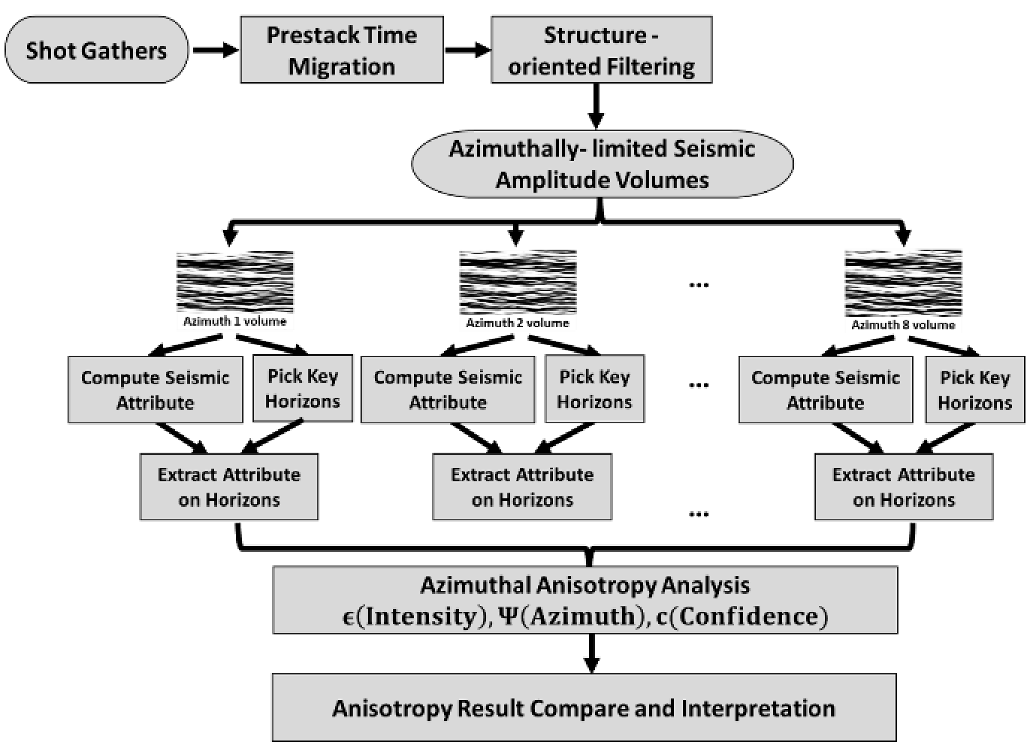

*Workflow for azimuthal anisotropy analysis and interpretation. Data should be preprocessed and then the target horizons are interpreted manually for each azimuthal volume in order to compensate the velocity anisotropy effect. Extracted attributed along key horizons were input for anisotropy analysis respectively. The output includes three key aspects of anisotropy: intensity, azimuth and confidence. (After Zhang et al., 2020).*

## Examples

### *AVAz applied to seismic amplitude*

The following example is from a survey acquired by Devon Energy in the Fort Worth Basin and described by Zhang et al. (2020). In this work, they extracted the amplitude and P-wave impedance on a suite of

picked or phantom horizons rather than in a window above the Viola hydraulic fracture barrier.

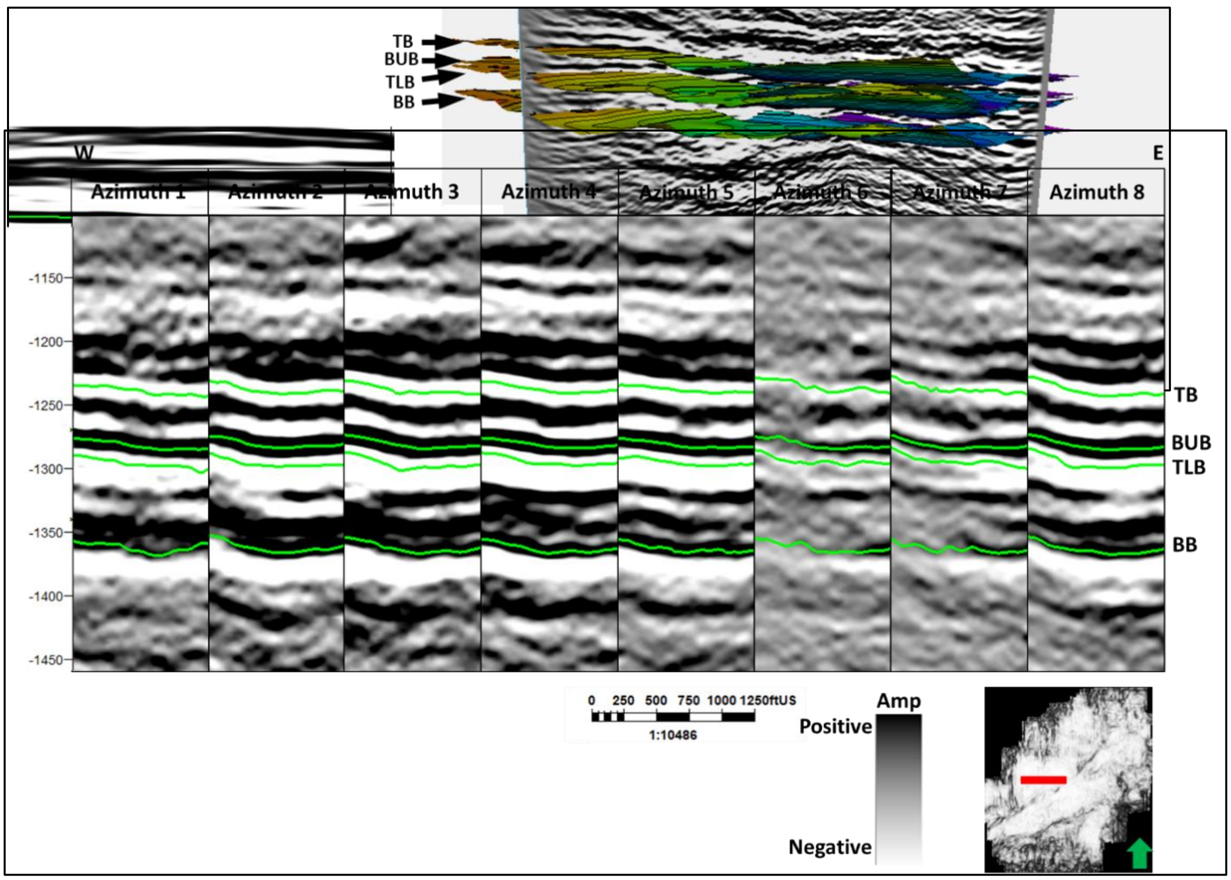


*Four key formation top horizons picked in the seismic survey, inline view on the left shows the thickness relationship of the upper Barnett, lower Barnett and Forestburg Lime, the right shows four interpreted horizons in 3D view. For each azimuthal volume, the horizons were picked separately. (After Zhang et al., 2020).*

*A vertical slice through a small part of the eight azimuthally migrated seismic amplitude volumes shown as a red line on the index figure in the lower right-hand corner. Note that amplitude varies by azimuthal volume and arrival time of four key horizons that are highlighted in green are different after manually interpreting the horizons. The* *interpretation uses 2D seed picking for each volume and QC manually afterward to minimize andy picking errors. (After Zhang et al., 2020).*

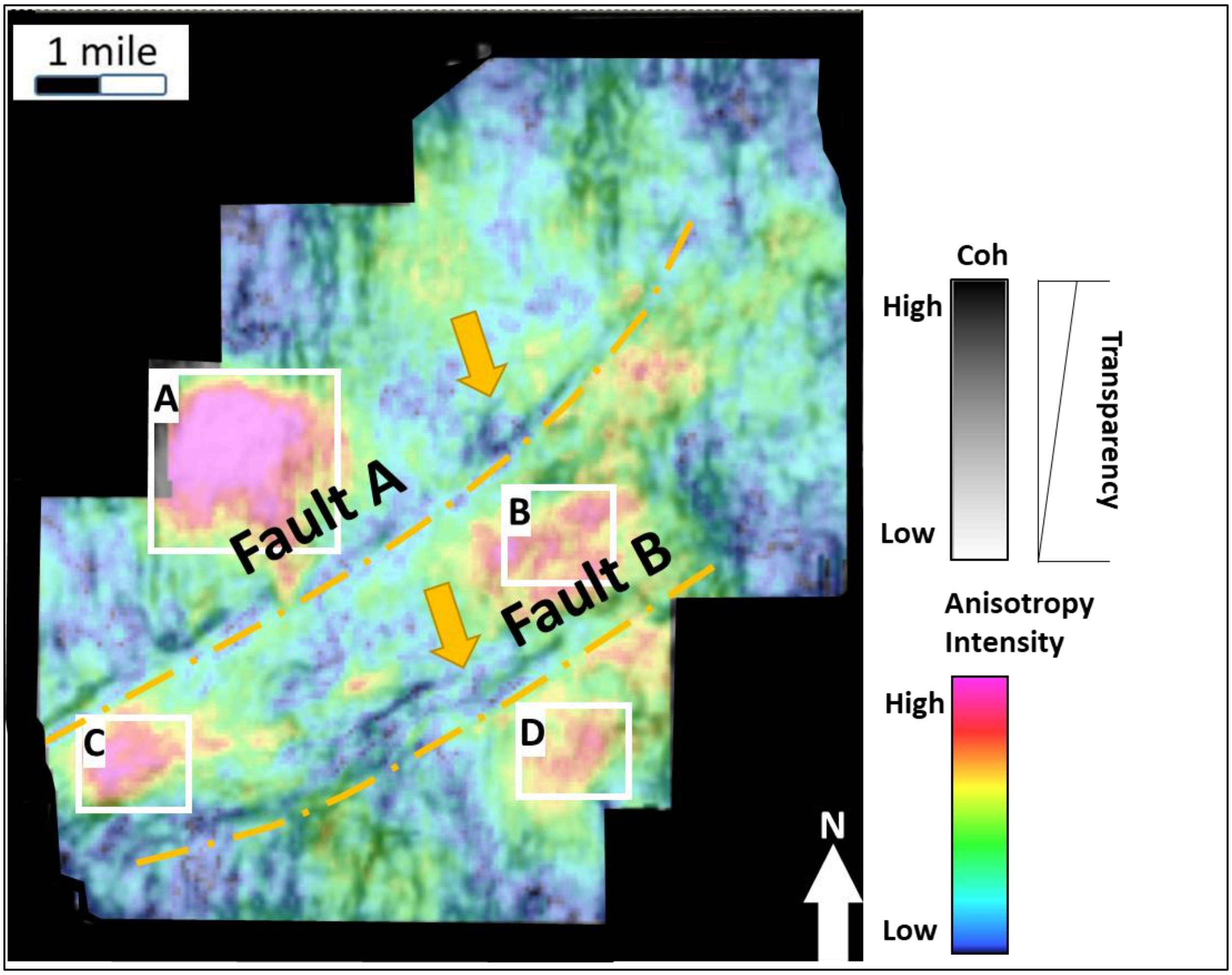


*A corendered image of coherence e and anisotropy intensity along the upper Barnett horizon near t=1.27 s. The anisotropy intensity map is from the Barnett top horizon anisotropy analysis. Four high anisotropy intensity zones have been identified as A, B, C, and D. High intensity zones correspond to low coherence area (lighter transparent area) which indicates the discontinuity is below the resolution of a typical seismic attribute. (After Zhang et al., 2020).*

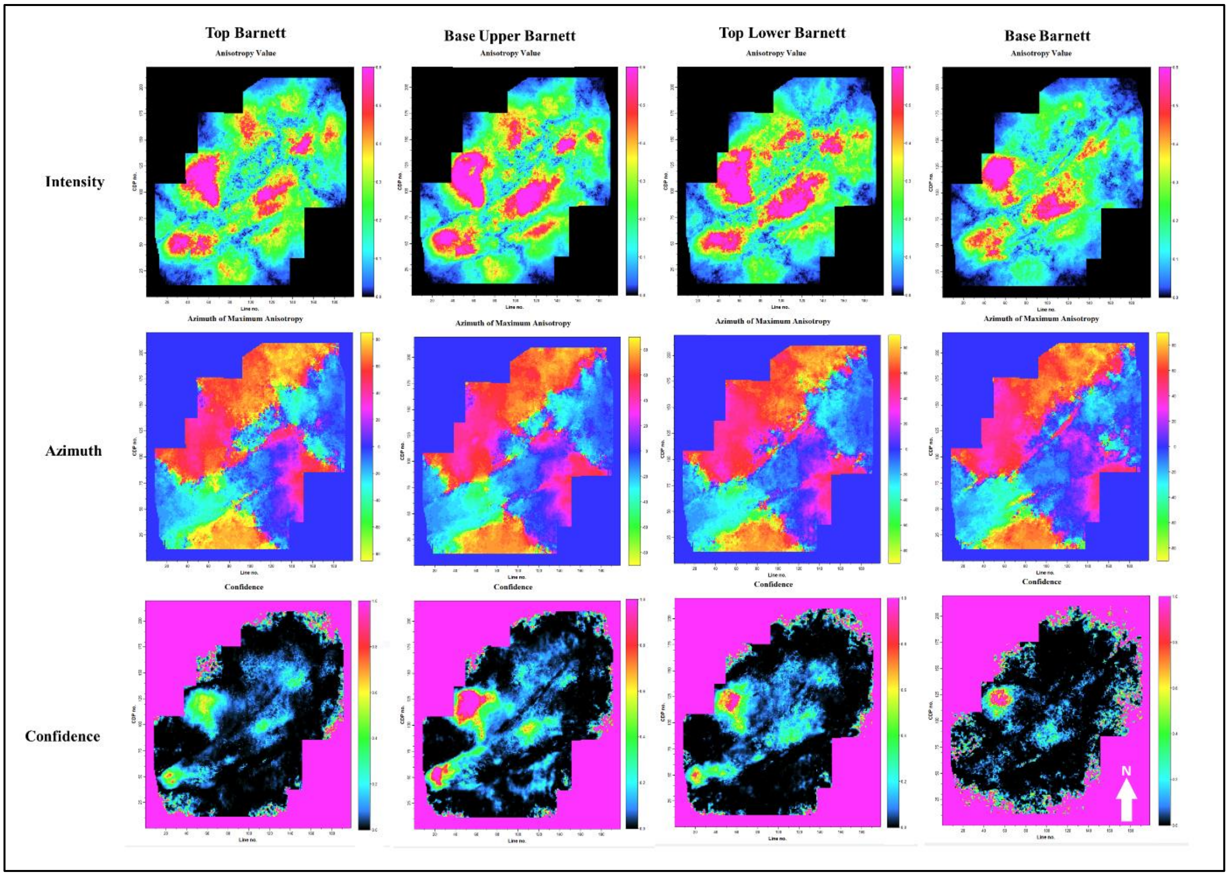


*Peak magnitude attribute anisotropy analysis result computed from the seismic amplitude volumes. The location of high anisotropy zone is the same with previous results. The azimuth of the high anisotropy zone is more consistent and less patchy than zones B and C. (After Zhang et al., 2020).*

## *Azimuthal anisotropy of P-impedance volumes*

P-impedance is the product of the P-wave velocity and the density. The density is a scalar value whereas the velocity can be anisotropic. For this reason, the P-impedance at different azimuths can vary, giving rise to azimuthal variations in the reflectivity. The previous images showed the anisotropy analysis of the azimuthally limited amplitude (reflectivity) volumes. Zhang et al. (2013) found that we can improve on these images by removing the impact of the seismic wavelet through poststack inversion of each of the azimuthally limited volumes. A different wavelet and different synthetic is used to tie each azimuthally limited volume, thereby removing the azimuthal changes in the source wavelet from the computation, and in principal, increasing the bandwidth of the data.

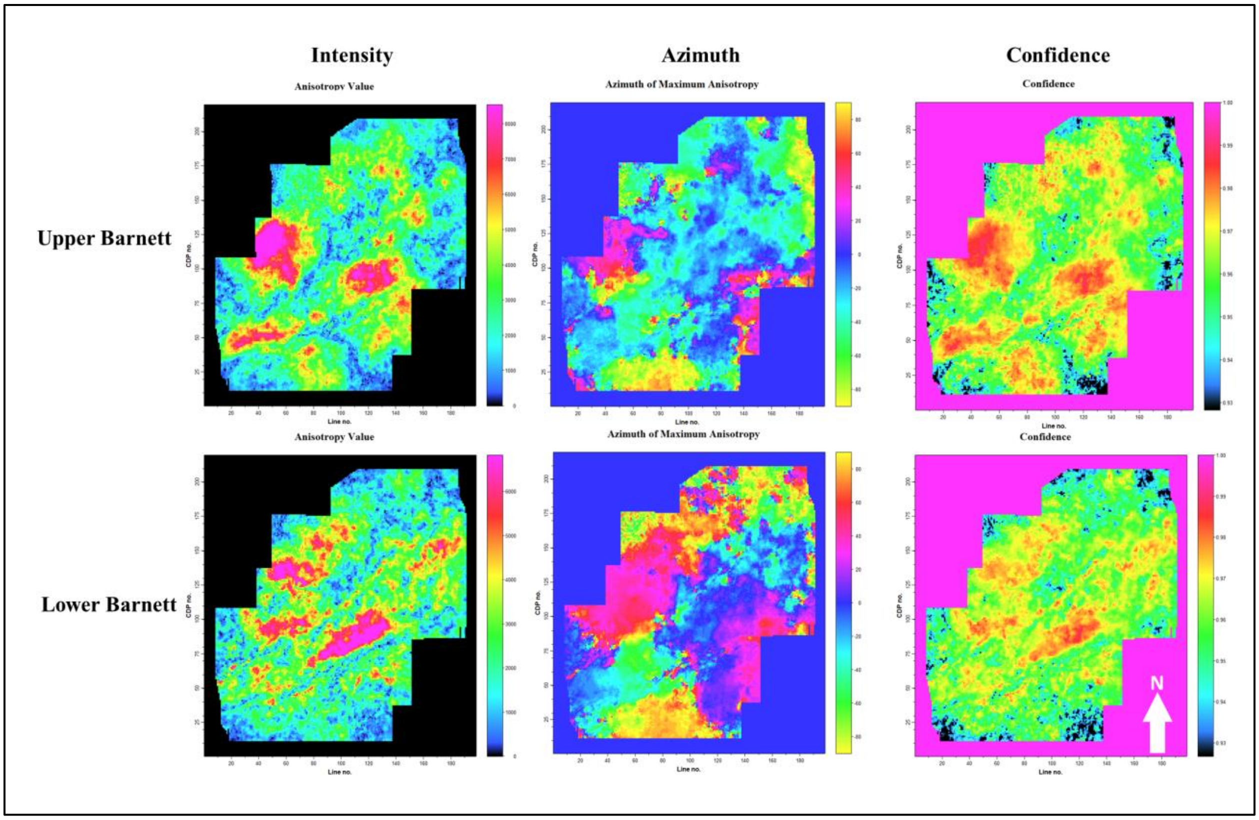


*P impedance anisotropy analysis result from two phantom horizons. Zone A, B and C are obvious to locate, but zone D is hard to locate on both surface and the lower Barnett, which generally have lower intensity of anisotropy than the upper Barnett Shale. (After Zhang et al., 2020).*

### *Azimuthal anisotropy of frequency and other attributes*

In addition to effecting P-wave impedance, azimuthal anisotropy will affect frequency, where the distance between the top and bottom of a thin bed will be slightly squeezed for higher velocities and stretched for lower velocities on prestack time-migrated data volumes. Lin et al. (2021) examine the effect of azimuthal anisotropy on several readily computed attributes:

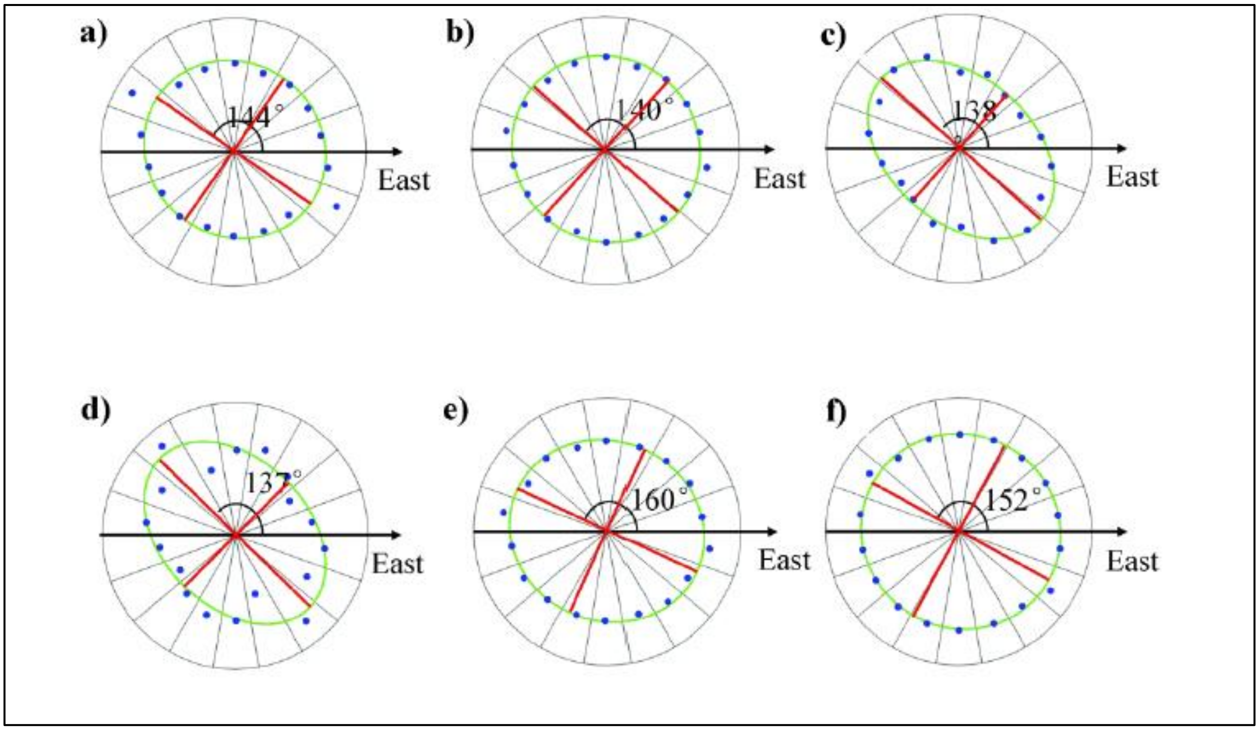


*The fitted anisotropic ellipsoids at the Well A location for the seismic parameters of (a) seismic root mean square (RMS) amplitude, (b) seismic maximum amplitude, (c) seismic amplitude, (d) seismic dominant frequency, (e) seismic instantaneous amplitude, and (f) seismic instantaneous frequency. (After Lin et al., 2021).*

### *Correlation of AVAz with the strike of curvature*

Azimuthal anisotropy may have a structural overprint, particularly near the tips of strike-slip faults (Bourne et al., 2000). Figure 93 shows the structural fabric of two surveys acquired in the Fort Worth Basin of north Texas. Figure 94 shows the corresponding AVAz vectors. Guo et al. (2016) find the same change in the azimuth of anisotropy on opposite sides of strike-slip faults that Bourne et al. (2000) found in outcrop and predicted through numerical modeling of stresses. Equally interesting is the fact that the southwest survey acquired prior to hydraulic fracturing exhibits intense anisotropy *e*, whereas the northwest survey acquired at 400 wells after hydraulic fracturing exhibits more subdued anisotropy, suggesting that hydraulic fracturing alters the velocity field.

The components of azimuthal anisotropy, $\varepsilon$ and $\psi$ define a vector that ranges between 0° and 180°. Guo et al. (2016) correlate this vector with the strike and orientation of structural curvature to determine if the structural deformation in someway controls the maximum horizontal stress. The following results were computed using program **aaspi_correlate3d**.

a)

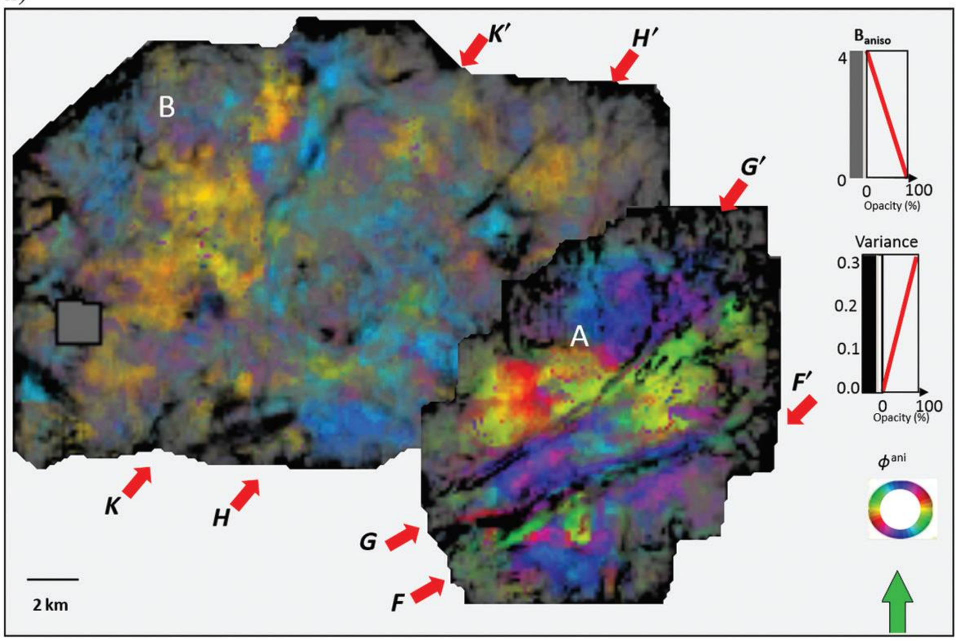


b)

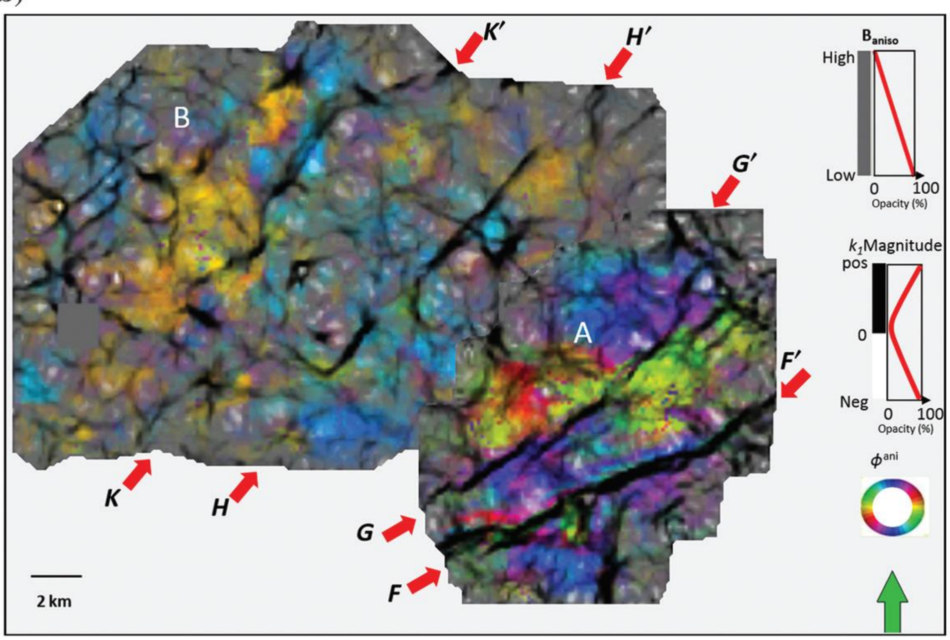


*Phantom horizon slices 20 ms above the top of the Viola Limestone through (a)* anisotropy strike ϕani modulated by its value Bani corendered by (a) variance and (b) most-positive curvature. The red arrows denote faults. *(After Guo et al., 2016)*

**a)**

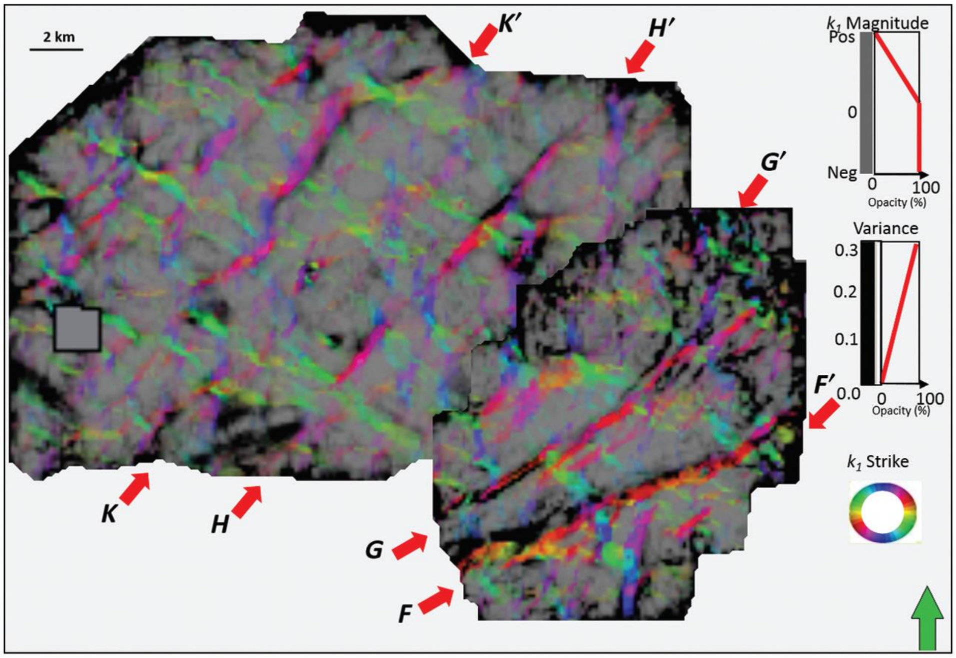


**b)**

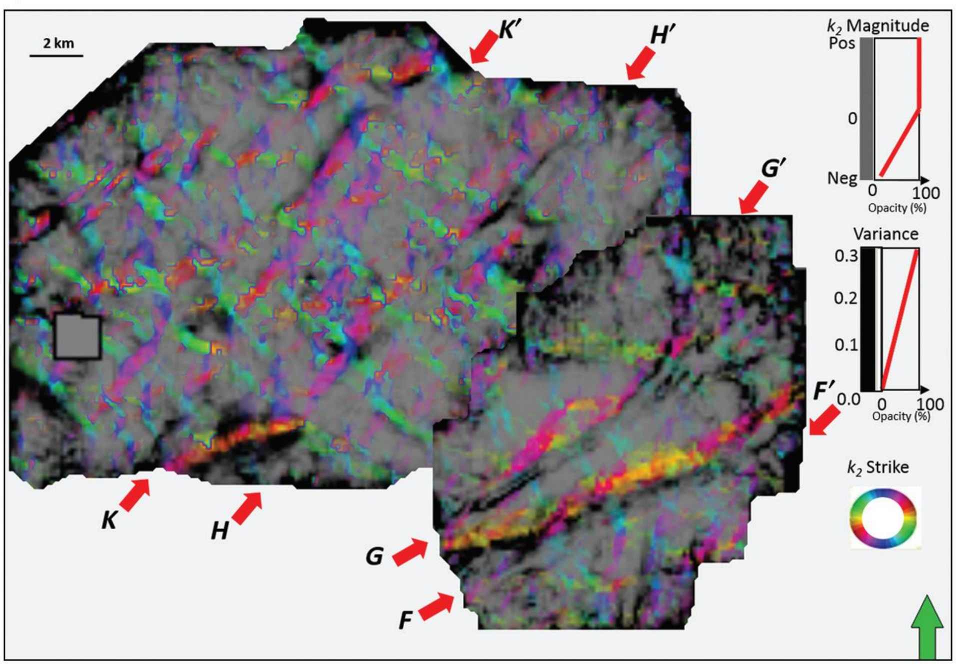


*Phantom horizon slices 20 ms above the top of the Viola Limestone through (a) $\psi_1$ (strike of most-positive curvature k1) modulated by $k_1$ corendered with variance, and (b) $\psi_2$ (strike of most-negative curvature $k_2$ modulated) by $k_2$ corendered with variance. The red arrows denote faults. (After Guo et al., 2016)*

**a)**

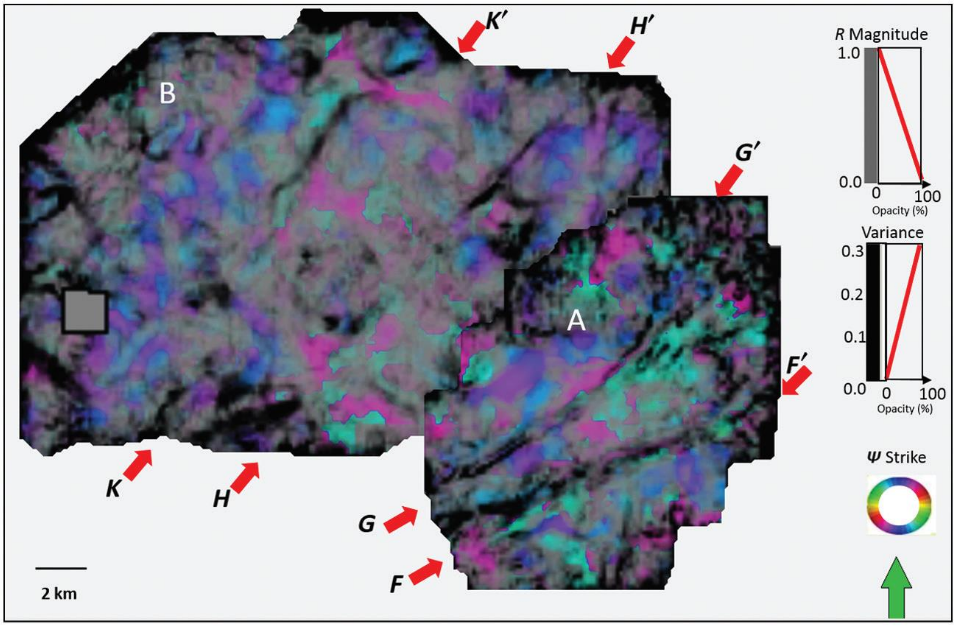


**b)**

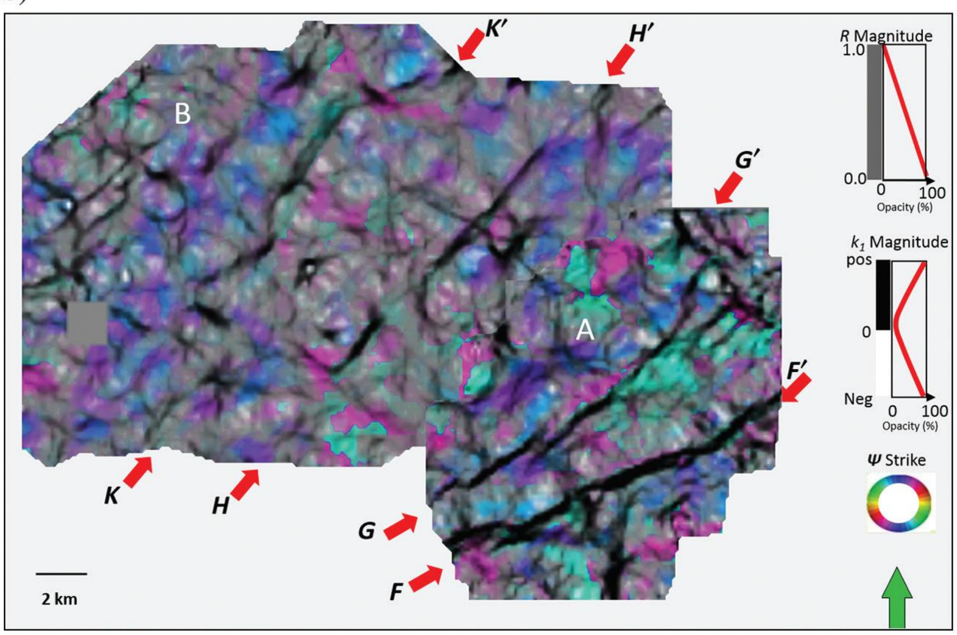


*Phantom horizon slices 20 ms above the top of the Viola Limestone through strike (Ψ) of new vector correlation (AVAz and $k_2$) modulated by its value (R magnitude) corendered by (a) variance and (b) most-positive curvature. The red arrows denote faults. (After Guo et al., 2016).*

## References

Bourne, S., F. Braukmann, L. Rijkels, B. Stephenson, A. Webber, and J. M. Emanuel, 2000, Predictive modeling of natural fractured reservoirs using geomechanics and flow simulation: Presented at 9th Abu Dhabi International Petroleum Exhibition and conference, ADIPEC 0911.

Guo, S., S. Verma, Q. Wang, B. Zhang, and K. Marfurt, 2016, Vector correlation of AVAz and curvature in a post hydraulically fracture Barnett Shale survey: Interpretation, **4**, SB23-SB35.

Ha, T., and K. J. Marfurt, 2017, Seismic reprocessing and interpretation of a fractured-basement play: Texas Panhandle: Interpretation, **5**, SK179-SK187.

Lin, K., B. Zhang, J. Zhang, H. Fang, K. Xi, and Z. Li, 2021, Predicting the azimuth of natural fractures and in-situ horizontal stress: A case study from Sichuan Basin, China: Geophysics, v, xx-yy

Perez-Altamar, R., and K. J. Marfurt, 2015, Identification of brittle/ductile areas in unconventional reservoirs using seismic and microseismic data: Applications to the Barnett Shale: Interpretation, **3**, T233-T243.

Qi, J., F. Li, and K. J. Marfurt, 2017, Multiazimuth coherence: Geophysics, **82**, P083–P089.

Rauch-Davies, M., and S. Randazzo, 2016, Poststack depth-impedance inversion over the Woodford Shale, Anadarko Basin: 86th Annual Intern

Rueger, A., 1997, P-wave reflection coefficients for transversely isotropic models with vertical and horizontal axis of symmetry: Geophysics, **62**, no. 3, 713–722, International Meeting, SEG, Expanded Abstracts, 3558–3562.

Zhang, J., J. Qi, Y. Zeng, K. Marfurt, and R. Slatt, 2020, Azimuthal anisotropy analysis applied to naturally fractured unconventional reservoirs: A Barnett Shale example: Interpretation, **8**, SP157-SP165.

Zhang, K., Y. Guo, B. Zhang, A. M. Trumbo, and K. J. Marfurt, 2013, Seismic azimuthal anisotropy analysis after hydraulic fracturing: Interpretation, **1**, SB27-SB36.